Structure of Na^+,K^+-ATPase at 11-Å Resolution: Comparison with Ca^{2+}-ATPase in E_1 and E_2 States

William J. Rice,* Howard S. Young,* Dwight W. Martin,† John R. Sachs,† and David L. Stokes*
*Skirball Institute of Biomolecular Medicine and Department of Cell Biology, New York University Medical Center, New York, New York 10016, and †Division of Hematology, Department of Medicine, State University of New York at Stony Brook, Stony Brook, New York 11794 USA

ABSTRACT Na^+,K^+-ATPase is a heterodimer of α and β subunits and a member of the P-type ATPase family of ion pumps. Here we present an 11-Å structure of the heterodimer determined from electron micrographs of unstained frozen-hydrated tubular crystals. For this reconstruction, the enzyme was isolated from supraorbital glands of salt-adapted ducks and was crystallized within the native membranes. Crystallization conditions fixed Na^+,K^+-ATPase in the vanadate-inhibited E_2 conformation, and the crystals had p1 symmetry. A large number of helical symmetries were observed, so a three-dimensional structure was calculated by averaging both Fourier-Bessel coefficients and real-space structures of data from the different symmetries. The resulting structure clearly reveals cytoplasmic, transmembrane, and extracellular regions of the molecule with densities separately attributable to α and β subunits. The overall shape bears a remarkable resemblance to the E_2 structure of rabbit sarcoplasmic reticulum Ca^{2+}-ATPase. After aligning these two structures, atomic coordinates for Ca^{2+}-ATPase were fit to Na^+,K^+-ATPase, and several flexible surface loops, which fit the map poorly, were associated with sequences that differ in the two pumps. Nevertheless, cytoplasmic domains were very similarly arranged, suggesting that the E_2-to-E_1 conformational change postulated for Ca^{2+}-ATPase probably applies to Na^+,K^+-ATPase as well as other P-type ATPases.

INTRODUCTION

The Na^+,K^+-ATPase generates Na^+ and K^+ gradients across the plasma membrane in virtually all animal cells and is a member of the P-type ATPase family of ion pumps (see Moller et al., 1996, for a recent review of P-type ATPases). During one enzymatic cycle, Na^+,K^+-ATPase transports three Na^+ ions out of the cell and two K^+ ions into the cell while hydrolyzing one molecule of ATP. This cycle also includes transient formation of a phosphoenzyme, which gives rise to the designation P type. Unlike other members of this family, Na^+,K^+-ATPase, along with the highly homologous H^+,K^+-ATPase, is a heterodimer composed of α and β subunits (Glynn, 1985). The α subunit consists of ~1020 amino acids and contains the sequence motifs that define the P-type family. Analysis of cDNA sequences of the α subunit shows that there are 10 transmembrane helices (M1–M10) that contain the cation binding sites. There are two cytoplasmic loops: a major loop between helices M4 and M5 that contains the nucleotide binding and phosphorylation sites and a minor loop between M2 and M3. On the extracellular side of the membrane, a small extracellular domain is composed of short loops between various transmembrane helices and contains the binding site for ouabain. The N-terminus of the β subunit forms a small intracellular domain followed by a short transmembrane helix and a large extracellular domain, which is composed of 250 residues with three sites of glycosylation. The β subunit is clearly required for proper folding and targeting of Na^+,K^+-ATPase to the plasma membrane, and may also influence enzymatic properties of the α subunit (Hasler et al., 1998; Abriel et al., 1999).

Early studies (Glynn, 1985) showed that Asp369 of Na^+,K^+-ATPase is phosphorylated from ATP when Na^+ is present. This phosphoenzyme cannot be hydrolyzed by water, but retains sufficient chemical energy to be able to transfer the phosphate to ADP, thus making ATP. Under different conditions, the enzyme can also be phosphorylated by P_i; the relatively low energy of this phosphoenzyme is suggested by its unreactivity with ADP, though it can be hydrolyzed by water in the presence of K^+. Because the same residue has been phosphorylated in both cases, the difference in reactivity has been explained by a structural difference in the protein. The high-energy phosphoenzyme was designated $E_1{\sim}P$ and the low energy phosphoenzyme E_2-P. Two analogous unphosphorylated species (E_1 and E_2) were subsequently identified, and a reaction cycle was proposed to define the causalities between ligand binding and conformational change:

$$E_1{\cdot}ATP + Na_i \leftrightarrow E_1 \sim P{\cdot}Na + ADP$$
$$\leftrightarrow E_2 - P + Na_o + K_o$$
$$\leftrightarrow E_2{\cdot}K + P_i + ATP \leftrightarrow E_1{\cdot}ATP + K_i,$$

where Na_i and K_i are intracellular ions, Na_o and K_o are extracellular ions, and P_i is orthophosphate. Similar mech-

Received for publication 21 August 2000 and in final form 2 February 2001.

Address reprint requests to Dr. David L. Stokes, NYU Medical Center, Skirball Institute 3-13, 540 First Avenue, New York, NY 10016. Tel.: 212-263-1580; Fax: 212-263-1580; stokes@saturn.med.nyu.edu.

0006-3495/01/05/2187/11 $2.00

anisms are consistent with experimental findings from other P-type ATPases, including Ca^{2+}-ATPase.

Subsequent to these thermodynamic investigations, the existence of the two major conformations of Na^+,K^+-ATPase was confirmed by various biochemical and biophysical techniques. For example, there are three major tryptic cleavage sites in the α subunit, and their sensitivity to cleavage depends on the conformational state (Jorgensen, 1975). Tryptic cleavage at the first site in the N-terminal tail blocked the transition from $E_1{\sim}P$ to E_2-P (Jorgensen and Klodos, 1978). Intrinsic tryptophan fluorescence is higher in E_2 than in E_1 conformations (Karlish and Yates, 1978), and fluorescence of probes such as fluorescein (Karlish, 1980) and iodoacetamidofluorescein (Kapakos and Steinberg, 1982), which bind to the α subunit, change dramatically at key steps in the reaction cycle. All of these changes were thought to reflect a global change in enzyme structure. More recently, changes in the pattern of iron-catalyzed oxidative cleavage (Goldshleger and Karlish, 1999; Patchornik et al., 2000) were interpreted in terms of particular domain movements associated with the E_1-to-E_2 transition. As a result of these and other experiments, it has been widely concluded that the conformational changes provide the mechanism of communication between cytoplasmic and transmembrane domains, thus coupling ATP hydrolysis to ion transport, though this conclusion is not universally accepted (Jencks, 1989).

The recently published atomic structure for Ca^{2+}-ATPase in the E_1 conformation and its comparison with the 8-Å structure in the E_2 conformation represents a major advance not only in defining pump architecture but also in specifying the structural basis for the E_2-to-E_1 transition (Toyoshima et al., 2000). Previous comparisons of 8-Å structures of *Neurospora* H^+-ATPase and rabbit muscle Ca^{2+}-ATPase from cryoelectron microscopy (Kühlbrandt et al., 1998; Stokes et al., 1999) provided a similar view of the conformational change, though specific assignment of the cytoplasmic domains was ambiguous at that time. With respect to Na^+,K^+-ATPase, although it was the first member of this family to be discovered (Skou, 1957) and the first to form two-dimensional (2D) crystals (Skriver et al., 1981), structural models have been limited to ~25-Å resolution (Mohraz et al., 1987; Skriver et al., 1992; Hebert et al., 1985, 1988), because of poor order, small crystal size, and the use of negative stain. Here we present a structure of E_2-state Na^+,K^+-ATPase from cryoelectron microscopy at 11-Å resolution, offering the first view of the entire heterodimer with unambiguous assignment of its domains. Comparison of our structure with E_2 and E_1 models of Ca^{2+}-ATPase indicates that the molecular architecture as well as the conformational changes from E_2 to E_1 are likely to be conserved across the P-type ATPase family.

MATERIALS AND METHODS

Protein isolation

Microsomes were prepared from supraorbital (or nasal) glands of salt-adapted immature ducks, according to Martin and Sachs (1999). Similar to their purification procedure, we used SDS to strip away peripheral membrane proteins, but longer tubular crystals were obtained at lower SDS: protein ratios (0.3 mg/ml SDS:1.4 mg/ml protein). Following SDS extraction, microsomes were centrifuged over a 10–50% sucrose step gradient. An opaque, protein-rich band was collected, from which the microsomes were pelleted by centrifugation and then were suspended in a solution containing 50 mM imidazole pH 7.5, 60 mM NaCl, 10 mM KCl, 0.5 mM EGTA, and 2.5% (w/v) sucrose.

Crystallization and data collection

Microsomes were crystallized at 1 mg/ml in 50 mM imidazole pH 7.5, 10 mM KCl, 2.5 mM $MgCl_2$, 0.5 mM EGTA, and 0.5 mM Na_3VO_4 on ice. Although not strictly required for crystallization, the orthovanadate species (prepared by boiling the stock solution for 10 min) seemed to stabilize the crystals and to increase the proportion of tubular crystals; in contrast, decavanadate solutions (prepared according to Stokes and Lacapere, 1994) provided only marginal improvement. Small amounts of detergent also aided crystallization, with 0.3–0.5 mg/ml diheptanoyl phosphatidylcholine (Kessi et al., 1994) being optimal. For data collection, a suspension of crystals was rapidly frozen in liquid ethane and imaged at ×50,000 magnification in the frozen-hydrated state with a Philips CM200 FEG electron microscope (Philips Electron Optics, Eindhoven, The Netherlands) operating at 200 kV with an Oxford CT3500 cryoholder (Oxford Instruments, Eynsham, UK). Electron micrographs of tubes were screened by optical diffraction, and well-ordered, tubular crystals were digitized at 14-μm intervals with a Zeiss SCAI microdensitometer (Carl Zeiss, Oberkochen, Germany).

Image analysis

The Fourier transform of a helical object comprises layer lines called $G_{nl}(R,Z_l)$ (Klug et al., 1958), which can be directly averaged if objects have the same helical symmetry. Real-space density maps are then determined by Fourier-Bessel transformation of $G_{nl}(R,Z_l)$ to yield $g_{nl}(r,Z_l)$, followed by summation of these $g_{nl}(r,Z_l)$ and Fourier transformation with respect to Z. The tubes of Na^+,K^+-ATPase showed much more variability in helical symmetry than Ca^{2+}-ATPase, which required us to employ a variety of averaging schemes, involving $G_{nl}(R,Z_l)$, $g_{nl}(r,Z_l)$ as well as real-space densities. Out of a total of 42 tubular crystals with 20 different helical symmetries, 27 tubular crystals spanning seven helical symmetries were chosen for structure analysis (Table 1). Within each helical symmetry, $G_{nl}(R,Z_l)$ were averaged and were used as a reference data set for correcting distortions of the individual tubes (Unwin, 1993; Beroukhim and Unwin, 1997). Where possible, overlapping repeats were chosen for distortion correction, thereby maximizing the number of molecules in the data set, even if this resulted in a non-integral number of repeats along a given tube. Defocus values were determined as previously described (Zhang et al., 1998), and the contrast transfer function of the microscope (CTF) was calculated based on 4.6% amplitude contrast, chosen because of the similarity of these tubular crystals to those of Ca^{2+}-ATPase (Toyoshima et al., 1993b). A weighted sum of $G_{nl}(R,Z_l)$ was calculated for each symmetry group, using CTF values for individual repeats as weights during averaging; these data were then corrected for the summed value of the CTF (Unwin, 1993). The crystals had p1 symmetry, and data obtained from the near and far sides of the tubes were kept separate during these and subsequent manipulations to allow for calculation of phase residuals and Fourier shell correlation coefficients (see Fig. 3).

TABLE 1 Summary of helical symmetries

Symmetry $(n_{1,0},n_{0,1})$*	Number of tubes	Number of repeats	Number of molecules	Unit cell (mean ± SE)		
				a (Å)	b (Å)	γ (°)
(−32,11)	3	4.00	5506	60.5 ± 0.5	67.6 ± 0.5	69.8 ± 0.2
(−33,11)	7	7.67	10964	61.3 ± 0.3	67.2 ± 0.2	70.3 ± 0.3
(−34,11)	3	3.20	6977	61.3 ± 0.3	67.2 ± 0.1	70.0 ± 0.2
(−38,13)	3	3.00	5111	61.0 ± 0.4	67.8 ± 0.2	70.2 ± 0.3
(35,11)	6	6.75	9902	61.1 ± 0.2	67.1 ± 0.3	68.5 ± 0.1
(36,11)	3	3.33	5669	61.0 ± 0.7	67.8 ± 0.5	68.4 ± 0.2
(37,11)	2	2.33	3157	60.7 ± 0.3	67.2 ± 0.1	68.8 ± 0.3
Sum	27	30.3	47286			

*Refers to the Bessel order or start number of the layer lines derived from the (1,0) and (0,1) directions of the underlying 2D lattice.

To combine the seven helical symmetries into a single map, we adopted recent strategies for aligning and averaging $g_{nl}(r,Z_l)$ (DeRosier et al., 1999). This technique was adopted because our initial data set consisted of 10 tubes with 10 different helical symmetries, thus preventing the standard averaging of $G_{nl}(R,Z_l)$ and making alignment of 3D structures for real-space averaging problematic. Collection of more micrographs expanded the population of several symmetry groups; nevertheless we found no improvement when we used real-space averaging, so we continued primarily with averaging of $g_{nl}(r,Z_l)$. As described by DeRosier et al. (1999), there is a direct correspondence of particular $g_{nl}(r,Z_l)$ for objects with the same underlying 2D lattice but different helical symmetries (defined by the start number (n) of the (1,0) and (0, 1) layer lines). Thus, the corresponding $g_{nl}(r,Z_l)$ can be averaged after adjusting the radial coordinate (R) for a systematic difference in tube diameter and for any slight magnification differences. This technique is valid only in cases where the unit cell is identical, and to be absolutely safe, we separated our seven symmetries into two groups, based on γ (Table 1). Tubes with γ of ~70.1° were scaled to match the reference symmetries characterized by $n_{1,0} = -32$ and $n_{0,1} = 11$, whereas symmetries with γ of ~68.5° were scaled to match the reference symmetry characterized by $n_{1,0} = 35$ and $n_{0,1} = 11$. This effectively divided the symmetry groups based upon the sign of $n_{1,0}$. It is unusual for the sign of the start number to vary among different helical symmetries, but in Na^+,K^+-ATPase crystals, the a axis of the unit cell is very nearly parallel to the meridional axis of the tubes. Thus, the corresponding helical family can be either right- or left-handed, depending on the circumferential vector that relates the 2D lattice to the helical lattice. This behavior has been previously observed in mutant bacterial flagellar filaments, which come in both left- and right-handed forms (Yamashita et al., 1998). To align the $g_{nl}(r,Z_l)$ data, we used a complicated procedure involving an inverse Fourier-Bessel transform of individual data sets to $G_{nl}(R,Z_l)$, which provided resolution-dependent phase statistics for determination of radial shift and relative magnifications. These manipulations required that the n and l values for $g_{nl}(r,Z_l)$ be systematically re-indexed to match the reference data set. Ultimately, the various $G_{nl}(R,Z_l)$ data sets were weighted according to the square root of the number of molecules they contained, were averaged, and finally were used to calculate 3D maps.

These procedures produced two independent 3D maps ($\gamma = 70.1°$ and 68.5°), which were aligned and averaged in real space. For alignment, the resolution was limited to 14 Å and maps were calculated at 1-Å intervals. Individual molecules were masked in each map, adjusted for density and magnification differences, and finally aligned by cross-correlation. These same alignment parameters were then applied to maps with 9-Å resolution, which were summed. For one measure of resolution, inverse Fourier-Bessel transforms were applied to averaged maps calculated from near-side and far-side data for calculation of their amplitude-weighted phase residual; another measure of resolution was based on Fourier shell cross-correlation (Miyazawa et al., 1999) from these same two data sets. Subtraction of background from $G_{nl}(R,Z_l)$ (Beroukhim and Unwin, 1997) was performed during intermediate alignment steps to ensure that data with high signal-to-noise ratio were used for alignment. However, we found that removal of low-amplitude data from the final map did not significantly improve its quality, as judged both by phase residuals and by correlation coefficients, so we chose to include all data out to 9-Å resolution for the final reconstruction.

These same real-space alignment procedures were used to compare Na^+,K^+-ATPase and Ca^{2+}-ATPase. In this case, the alignment included only the cytoplasmic domains after trimming off the decavanadate peak that is unique to Ca^{2+}-ATPase (see Results). After alignment, the correlation coefficient between these cytoplasmic regions was 0.84, which compares favorably with the value of 0.90−0.95 routinely obtained between independent structures of Ca^{2+}-ATPase.

Docking of atomic coordinates to electron density maps

We used the automated docking package Situs (Wriggers et al., 1999) to fit the atomic coordinates of Ca^{2+}-ATPase (accession code 1EUL, Toyoshima et al., 2000) to the Na^+,K^+-ATPase electron density map. We initially tried using the flexible docking procedure described by Wriggers et al. (2000), but this procedure led to an unacceptable loss of secondary structure in the atomic coordinates of Ca^{2+}-ATPase. We therefore divided these coordinates into four domains (N, P, nose, and transmembrane) and used the Situs 1.3 package for rigid-body docking into the corresponding regions of the density map. Both the nose and P domains were optimally described by four code-book vectors, whereas the N domain was best described by five code-book vectors. A density threshold was applied to the map corresponding to 20% of its maximum density; however, the results were not sensitive to this level (the threshold for Fig. 5 is ~25%). Atomic coordinates with a temperature factor above 90 were not considered in the fitting, because these are likely to represent disordered regions in the density map. Fitting the P domain was attempted before and after removing the extra density (asterisk in Fig. 5 *C*), but ultimately we could not obtain a unique fit (see Results). This same process was used to dock the atomic coordinates to the 8-Å Ca^{2+}-ATPase electron density map (Zhang et al., 1998), except that the high-density peak corresponding to decavanadate was removed. To quantitate the fit, Situs calculates both RMS deviation of code-book vectors and correlation coefficients after generating density maps from the fitted coordinates. In our case, the fitted domains were reassembled into a single set of atomic coordinates, and Situs then required another round of rigid-body docking before calculating these parameters. For this final fit, we specified only three code-book vectors for the entire molecule to prevent any further reorganization of the domains.

RESULTS AND DISCUSSION

Crystallization and structure determination

For crystallization, we used native microsomes from duck supraorbital glands (Martin and Sachs, 1999) and buffer conditions that were discovered almost 20 years ago (Skriver et al., 1981). These conditions include orthovanadate, which inhibits most if not all P-type ATPases by mimicking the transition state for phosphorylation-dephosphorylation in the E_2 state (Cantley et al., 1978). However, we found that although orthovanadate increased the proportion of crystalline material, it was not absolutely essential for crystallization. This suggests that the stabilization of the E_2 conformation by K^+ and Mg^{2+} may be the key to crystallization. Indeed, stabilization of E_2-P with ouabain prevented crystallization altogether. A similar conclusion was reached for Ca^{2+}-ATPase crystals, which require EGTA and decavanadate; thapsigargin forms a dead-end complex with Ca^{2+}-ATPase in the E_2 conformation and thus dramatically stabilizes these crystals (Sagara et al., 1992; Stokes and Lacapere, 1994).

Our Na^+,K^+-ATPase crystals adopted a wide variety of morphologies (Fig. 1), but tubular crystals were chosen for analysis because their helical symmetry offered a convenient means of determining 3D structure (DeRosier and Moore, 1970). Unlike flat 2D crystals, these tubular crystals do not require tilting, and the resulting resolution is isotropic due to their inherent cylindrical symmetry. Images of tubular crystals in the frozen hydrated state were recorded and the underlying helical symmetry was characterized by assigning Bessel orders to the primary layer lines composing the Fourier transform (Fig. 2). A total of 27 tubes falling into seven helical symmetries were used for our reconstruction (Table 1). We used standard techniques for Fourier space averaging within each helical symmetry. The symmetry groups were divided into two parts based on their unit cells, and Fourier-Bessel components were averaged within these groups (DeRosier et al., 1999). Density maps were then calculated for both unit cells, and real-space averaging was used to generate the final structure. Measures of phase residuals and correlation coefficients are shown in Fig. 3; although phase residuals are better than random and there is positive correlation all the way to 9 Å, our inability to resolve any α helices (e.g., transmembrane helices) suggests that the effective resolution is somewhat worse than 10 Å. At 11 Å, the phase residual (62°) and correlation coefficient (0.37) compare favorably with the corresponding values (60° and 0.3) reported by Miyazawa et al. (1999) for tubular crystals of the nicotinic acetylcholine receptor.

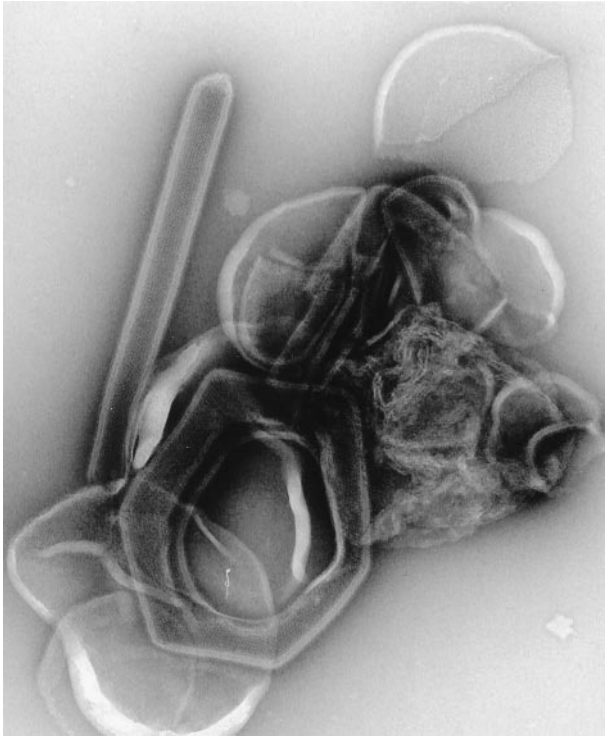

FIGURE 1 Negatively stained crystals of Na^+,K^+-ATPase. Most of the vesicles contained ordered arrays and many developed distorted corners reflecting the underlying arrays. A small proportion of vesicles elongated into tubes ~800 Å in diameter, which contained a helical array of Na^+,K^+-ATPase molecules.

Orientation in the membrane

The orientation of Na^+,K^+-ATPase in the membrane can be deduced from cross sections through the tubes (Fig. 4 *A*). The membrane appears as two discontinuous regions of high density that circumnavigate the section, and individual molecules appear to protrude from both sides of this membrane. The membrane borders are more precisely defined by circumferentially averaging the mass distribution across the tube, and the resulting profile (Fig. 4 *B*) reveals two peaks corresponding to electron-dense phosphates from the lipid headgroups. This high scattering density also results in low contrast and consequent blurring of the molecule at the membrane borders. Both the cross section and the averaged mass distribution show that the majority of the molecular mass is located inside the tube, with a smaller mass on the outside. This is opposite to the tubular crystals of Ca^{2+}-ATPase, in which most of the mass, corresponding to the cytoplasmic domain, is located outside of the tube (Toyoshima et al., 1993a). Nevertheless, if the Ca^{2+}-ATPase profile is inverted, it closely resembles that of the Na^+,K^+-ATPase, except for the smaller extra density on the outside of the Na^+,K^+-ATPase tubes (Fig. 4 *B*). This implies that internal densities in the Na^+,K^+-ATPase tubes correspond to the cytoplasmic domains and external densities to the β subunit. These assignments are consistent with ATPase activity measurements of microsomes before crystallization, which require detergent permeabilization for full activity (Martin and Sachs, 1999; our unpublished data). Also, when a single molecule from the map is contoured to correspond

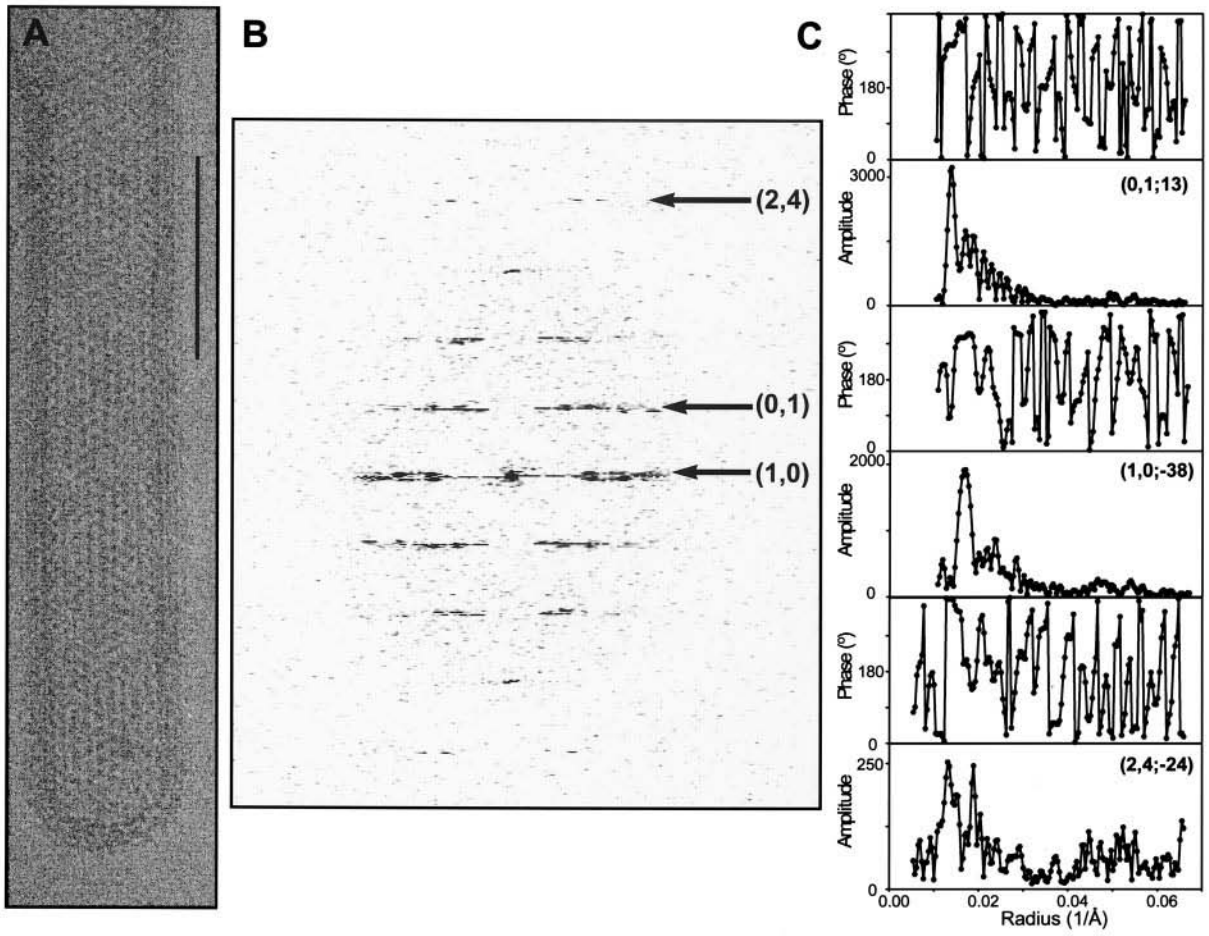

FIGURE 2 Image and Fourier data for a frozen-hydrated tube. (*A*) Electron micrograph of a tubular crystal embedded in amorphous ice at −180°C. Scale bar, 100 nm. (*B*) The calculated diffraction pattern of the tube is composed of a set of layer lines, three of which have been indexed according to the Miller indices (*h*, *k*) of the underlying 2D lattice. Layer lines as high as (2, 4) were often visible, corresponding to approximately 1/16-Å resolution. (*C*) Amplitudes and phases for layer lines labeled in *B*, which are consistent with p1 symmetry. Amplitude units are arbitrary but indicate the relative intensities of layer line data. Each layer line is labeled according to an (*h*, *k*) index and helical start number (*n*).

to the appropriate molecular mass of 147 kDa, 54% is inside the tube, 23% is within the membrane, and 23% is outside the tube, which is consistent with predictions based on a 10-transmembrane helix α-chain model (58%, 17%, and 25%, respectively; Moller et al., 1996). The overestimate in the percentage within the membrane is likely to be a consequence of the low contrast at the membrane boundary. Carbohydrate groups, which are heterogeneous and likely to be disordered, were not included in these predicted sizes.

Overall shape of Na^+,K^+-ATPase

The molecular envelope of the reconstructed Na^+,K^+-ATPase is shown in Fig. 5. On the cytoplasmic side of the membrane, the Na^+,K^+-ATPase α subunit consists of a stalk just above the membrane, which is connected to a tripartite head extending ~75 Å above the membrane. Generally speaking, this structure is consistent with previous reconstructions of Na^+,K^+-ATPase (Mohraz et al., 1987; Skriver et al., 1992; Hebert et al., 1985, 1988), but with more clearly defined domains and membrane topology. The cytoplasmic headpiece is reminiscent of that from Ca^{2+}-ATPase in the E_2 conformation, which consists of a highly conserved phosphorylation domain (P) sitting on top of a narrow stalk with a nose pointing to one side and a nucleotide-binding domain (N) above (Toyoshima et al., 2000). Two notable differences are a cleft that separates the nose from the N-domain and a protrusion on top of the P-domain (Fig. 5 *C*, *asterisk*). This protrusion is involved in a strong crystal contact with the N-domain of the adjacent molecule (Fig. 5 *C*, *arrow*) and the cleft corresponds to a very high density in the Ca^{2+}-ATPase map, which has been associated with an intramolecular site for decavanadate (Stokes and Green, 2000; Toyoshima et al., 2000). The location of this site at the intersection of the three main cytoplasmic domains together with the polyanionic nature of decavanadate

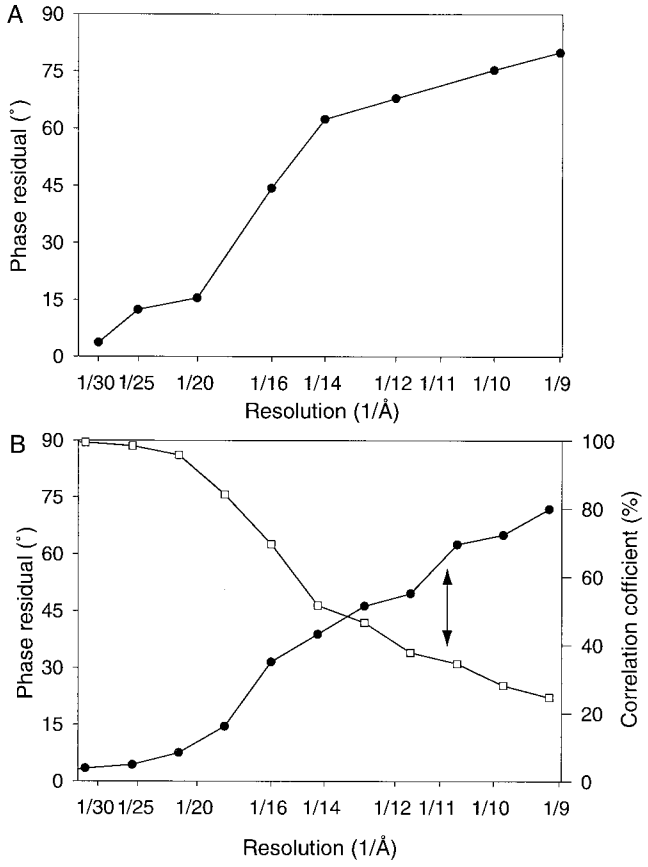

FIGURE 3 Statistics of data averaging. (*A*) Amplitude-weighted phase residuals between independent near and far data sets were calculated from Fourier data. A phase residual of 90° is expected from random data. (*B*) Fourier shell correlations were calculated from 3D maps derived from the near and far data sets according to Miyazawa et al. (1999). This procedure produces both phase residuals (●) and correlation coefficients (■).

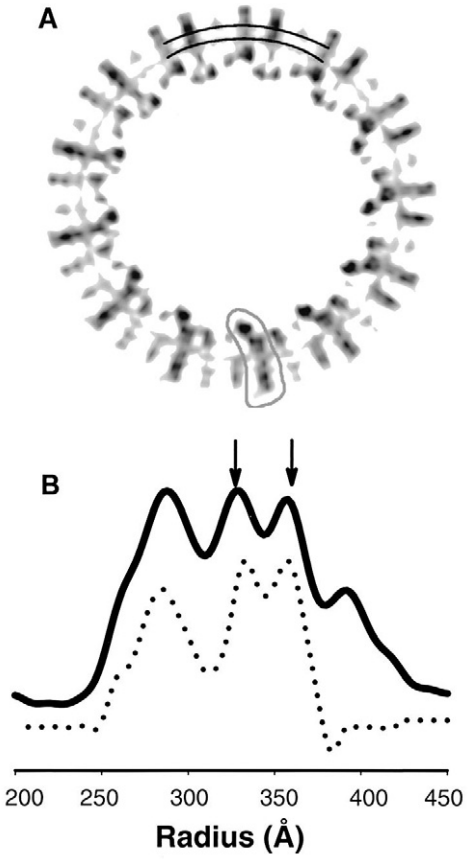

FIGURE 4 Mass distribution across the membrane. (*A*) Cross section through a reconstructed tube shows 13 Na^+,K^+-ATPase molecules are arranged around the tube, reflecting the dominant 13-start helices indexed as (0, 1). One molecule is circled, and the membrane boundaries are highlighted with black lines at the top of the figure. (*B*) Average radial density distribution of Na^+,K^+-ATPase (*solid line*) is compared with that of Ca^{2+}-ATPase (*dotted line*). A good match was obtained after inverting the Ca^{2+}-ATPase profile and aligning the phosphate headgroups delineating the membrane (*arrows*). Thus, the broader peak at low radius corresponds to the cytoplasmic domain, and the smaller peak at high radius, which is not present in Ca^{2+}-ATPase, corresponds to the β subunit.

raised the possibility that decavanadate was artificially holding the cytoplasmic domains together. In contrast, the x-ray structure of the E_1 state revealed that these same domains have very little interaction and have undergone large inclinations and rotations (20°–90°) relative to the EM structure of the E_2 state. Nevertheless the rather similar spatial arrangement of these cytoplasmic domains in the current structure of Na^+,K^+-ATPase suggests that their more compact organization is characteristic of a native E_2 conformation.

The transmembrane domain of Na^+,K^+-ATPase is narrow in the middle of the membrane but widens at the two membrane surfaces, giving it an hourglass shape. This widening is also apparent in lower-resolution maps of Ca^{2+}-ATPase (Toyoshima et al., 1993a; Yonekura et al., 1997) and can be partly explained by the lower contrast inherent at the membrane boundaries. On the extracellular side of the membrane, Na^+,K^+-ATPase forms a dense globular structure that is mostly composed of β subunit, which is discussed in more detail below.

Comparison with Ca^{2+}-ATPase

Our map of Na^+,K^+-ATPase was aligned with that of Ca^{2+}-ATPase by using cross-correlation to fit the cytoplasmic regions of the two molecules (Fig. 5). Cross sections through the aligned maps show that their phosphorylation (P) domains, which include most of the highly conserved sequences, are virtually superimposable and that the other two cytoplasmic domains (N and nose) are of comparable shape and size (Fig. 6, *A* and *B*), though the N-domain is slightly displaced due to its different tilt (Fig. 5 *F*). Other differences include the decavanadate density for Ca^{2+}-ATPase and an extra lump on the P-domain of Na^+,K^+-ATPase (V_{10} and *asterisk* in Fig. 6 *B*, respectively). As mentioned, the cleft between the N-domain and the nose of Na^+,K^+-ATPase is primarily due to the absence of the

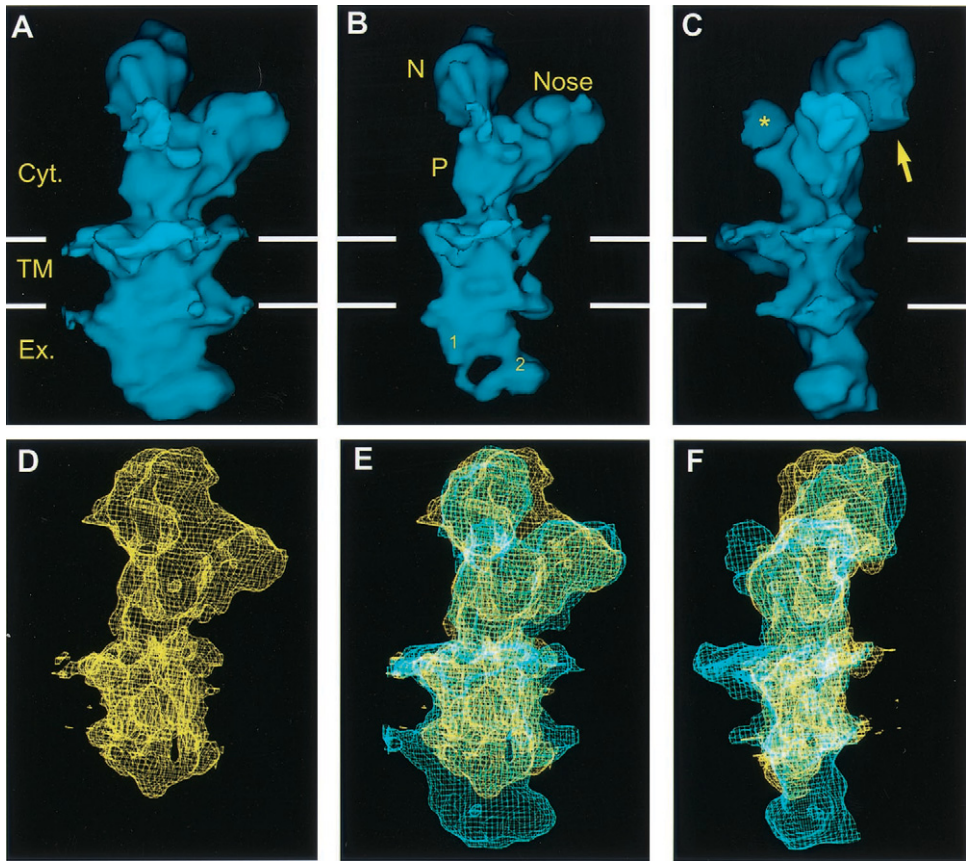

FIGURE 5 A 3D reconstruction of Na^+,K^+-ATPase and alignment with Ca^{2+}-ATPase. (*A–C*) Two views of Na^+,K^+ ATPase at 11-Å resolution, with *A* and *C* related by a 90° clockwise rotation and *B* plotted at a higher density threshold. The cytoplasmic head is subdivided into three parts: nose and P- and N-domains. A protuberance from the P-domain (*) is involved in a crystal contact with the N-domain of a neighboring molecule (contact site indicated by the *arrow*). The membrane domain is delineated by the horizontal white lines. (*D–F*). Na^+,K^+-ATPase has been aligned with Ca^{2+}-ATPase (yellow) showing a generally similar disposition of the domains. Extra densities on the bottom of Na^+,K^+-ATPase and at the cytoplasmic membrane surface are likely attributable to the β subunit. In *B*, 1 and 2 indicate regions of contact between α and β subunits, which are near loops between M7/M8 and M3/M4 of the α subunit (see Fig. 7 *D*). Solid surface renderings were prepared with the Advanced Visual Systems software suite (Waltham, MA) and fishnet renderings with the program O (Jones et al., 1991). Alignment was done by cross-correlation between the cytoplasmic domains of the two molecules. The surfaces correspond to ~75% of the expected molecular volume, except in *B*, which is ~50%.

decavanadate density, but is enhanced by the greater distance between nose and N-domains. Although this difference is relatively minor, it illustrates the flexibility of these domains, even in this particular E_2 conformation. The membrane region was generally similar, though unlike the electron microscopy maps of Ca^{2+}-ATPase and H^+-ATPase, our map for Na^+,K^+-ATPase did not define individual transmembrane helices. As a result, the gap between these helices that was previously postulated to form a water-filled channel from the extracellular surface (Zhang et al., 1998; Gadsby et al., 1993) could not be resolved. Nevertheless, the molecular envelope in the middle of the membrane suggests that the arrangement of helices in Na^+,K^+-ATPase is very similar to Ca^{2+}-ATPase and H^+-ATPase, though rotated a few degrees clockwise relative to the P-domain (Fig. 6, *D* and *E*).

The transmembrane location of the β subunit is suggested by extra density at the cytoplasmic and extracellular membrane surfaces, though corresponding extra density is not directly visible in the middle of the membrane. In particular, there is considerable extra density at the cytoplasmic surface (left side of Fig. 5 *F* and bottom of Fig. 6 *D*), which is most likely to correspond to the N-terminus of the β subunit and which is consistent with extra density in a similar location on the extracellular side of the membrane (Fig. 5 *E*). These observations suggest that the membrane-spanning helix of the β subunit passes close to M7 and M10, perhaps interacting with the C-terminus or the M6/M7 loop of the α chain in the cytoplasm. On the extracellular side, interactions between β and the M7/M8 loop of α are well established (Lemas et al., 1994; Colonna et al., 1997) and have been specifically localized to the portion of β that is close to the extracellular membrane surface. In fact, the extracellular part of β appears to be divided into two parts: residues 60–112, which are near the membrane surface and are predicted to have a significant amount of secondary struc-

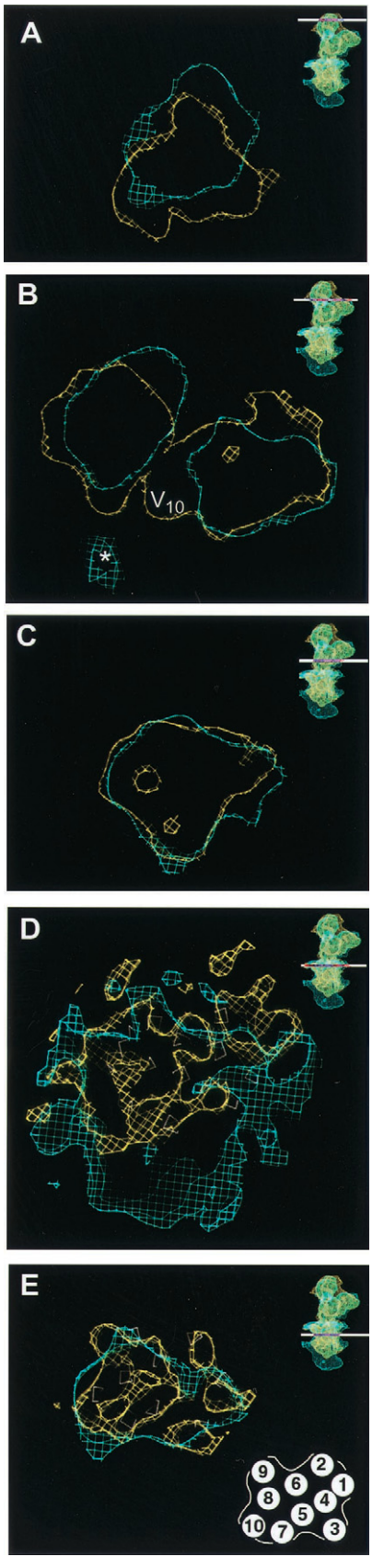

FIGURE 6 Cross sections through the aligned Na^+,K^+-ATPase and Ca^{2+}-ATPase molecules shown in Fig. 5. (*A*) The shape of the N-domain is well conserved, though the entire domain is shifted. (*B*) V_{10} indicates the decavandate binding site between the N-domain and the nose on Ca^{2+}-ATPase, and the asterisk indicates the protuberance from the P-domain of Na^+,K^+-ATPase (seen also in Fig. 5). (*C*) The shape of the P-domain is exceedingly well conserved, which is consistent with its high degree of sequence homology. (*D*) The cytoplasmic membrane surface of Na^+,K^+-ATPase has extra density on the bottom, which likely corresponds to the N-terminal part of the β subunit. This region is noisier due to the presence of the lipid phosphates. (*E*) The inset indicates the position of transmembrane helices in Ca^{2+}-ATPase together with their sequence based on the x-ray structure. The level of each section is indicated by the bar across the inset on the upper right of each panel.

ture, and residues 125–302, which have little predicted secondary structure but contain the three disulfide bonds and three glycosylation sites. Indeed, when our map is displayed at a high-density cutoff (Fig. 5 *B*), the β subunit appears as two discrete densities connected by a narrow loop. The portion closer to the membrane (labeled 1 in Fig. 5 *B*) is well positioned to interact with the M7/M8 loop of α, whereas the distal portion of β is larger and less intimately associated with this M7/M8 loop. Nevertheless, this distal portion does appear to contact the α subunit near the M3/M4 loop (contact labeled 2 in Fig. 5 *B*) and potentially to cover the putative, water-filled cavity leading to the ion-binding sites.

Fitting of Ca^{2+}-ATPase coordinates

To further aid our modeling of Na^+,K^+-ATPase, we employed both manual and automated docking of atomic coordinates to electron density maps. We started by dividing the atomic coordinates for the E_1 state of Ca^{2+}-ATPase (PDB accession code 1EUL) into three parts (nose, P-, and N-domains) and then did the same for the electron density map of Na^+,K^+-ATPase. We then used Situs 1.3 (Wriggers et al., 1999, 2000) to dock each of the three domains individually by rigid-body movement. For the N-domain and nose, we were able to choose between several equally likely fits based on the connectivity of the N- and C-termini with other parts of the molecule. However, fitting of the P-domain produced 12 different models with equivalent correlation coefficients, probably due to the symmetrical shape of this region and the extensive editing at domain interfaces before docking. When these same procedures were applied to the 8-Å Ca^{2+}-ATPase map, the higher resolution and fidelity of sequence produced unique fits for all three domains (manuscript in preparation). Furthermore, the resulting model visually resembled that described by Toyoshima et al. (2000). We therefore docked the P domain manually into our Na^+,K^+-ATPase map, using our fitting to the Ca^{2+}-ATPase map as a guide. The resulting fit (Fig. 7) is characterized by a correlation coefficient of 0.601, compared with a value of 0.623 for automated docking to the Ca^{2+}-ATPase map.

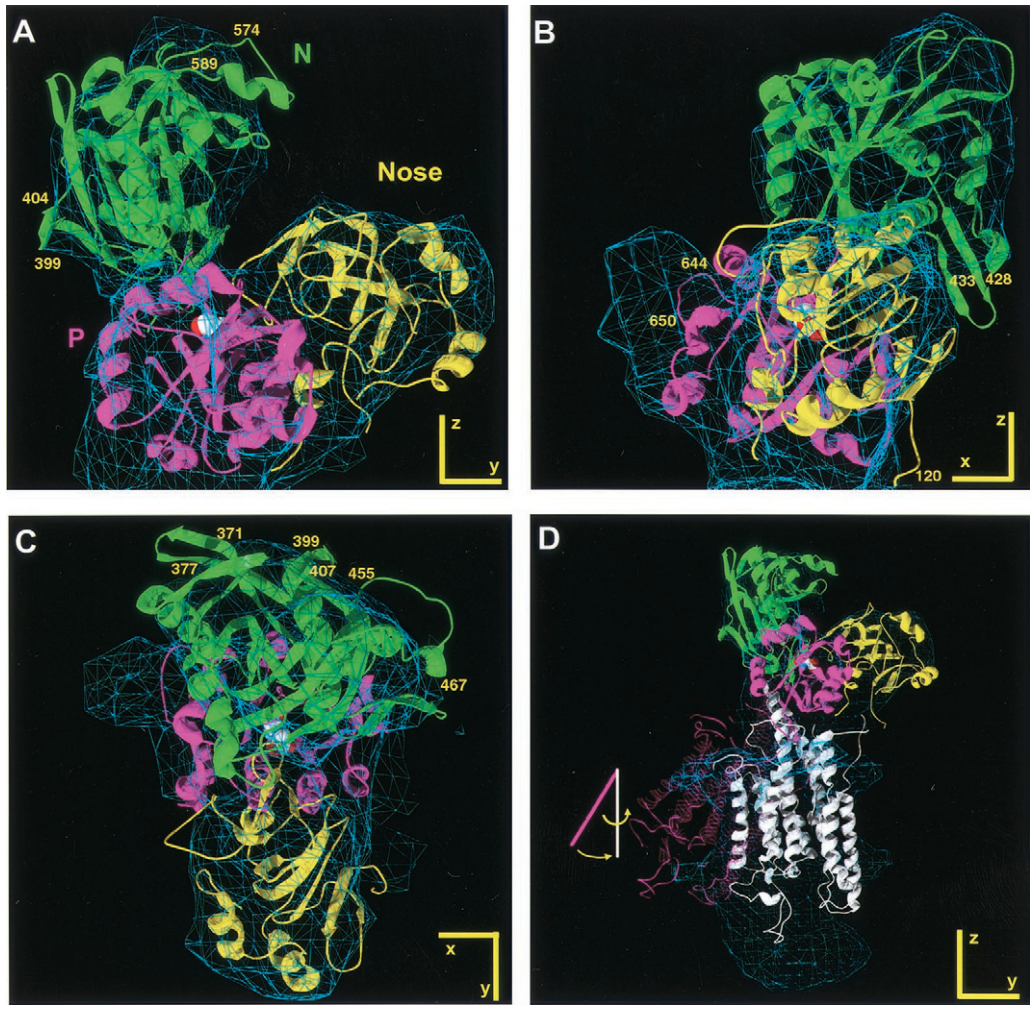

FIGURE 7 Fitting of Ca^{2+}-ATPase coordinates in the E_1 conformation to the map of Na^+,K^+-ATPase in the E_2 conformation. Automated docking of atomic coordinates to electron density maps was performed using the program Situs 1.3 (Wriggers et al., 1999). Each cytoplasmic domain was separately docked to the corresponding region of Na^+,K^+-ATPase. The side chain of Asp351 of Ca^{2+}-ATPase, which is analogous to Asp369 of Na^+,K^+-ATPase and is phosphorylated by ATP, is shown as a white space-filling model. (*A–C*) Three different views of the cytoplasmic domains with protruding surface loops identified according to their Ca^{2+}-ATPase sequence. (*D*) Side view of the entire molecule illustrating the relationship of the transmembrane domain to these cytoplasmic domains. The magenta ribbon corresponds to the location of these helices after rigid-body fitting of the P-domain into the Na^+,K^+-ATPase map. The white ribbons illustrate a more reasonable fit to the density map. This suggests an ~40° inclination and ~30° rotation of the P-domain relative to the transmembrane domain during the E_2 to E_1 conformational change. The figure was created with Swiss PDB viewer (http://expasy.cbr.nrc.ca/spdbv) with the final rendering done by POVray (http://www.povray.org).

Visual inspection of the docked coordinates showed that various surface loops from the Ca^{2+}-ATPase coordinates fit poorly within the Na^+,K^+-ATPase map. In contrast, the Ca^{2+}-ATPase map generally had bulges that accommodated these loops (not shown). By referring to a recent sequence alignment (Stokes and Green, 2000), we found that the badly matched loops could all be explained by variations in the amino acid sequences of Ca^{2+}-ATPase and Na^+,K^+-ATPase. In particular, the prominent protrusion from the P-domain of Na^+,K^+-ATPase is close to the variable loop between residues 644 and 650 in Ca^{2+}-ATPase, which is followed by an insertion of 20 amino acids in the Na^+,K^+-ATPase sequence (after Glu635 of Na^+,K^+-ATPase); the size of this insertion is consistent with the size of the extra density. In the crystals, this region contacts the N-domain of adjacent molecules, tempting us to speculate that this loop might mediate the self-association of α subunits, which has previously been attributed to the sequence Arg554-Pro785 (Koster et al., 1995).

To explain the loops that protrude from the Na^+,K^+-ATPase density (Fig. 7), this same sequence alignment predicted deletions from Ca^{2+}-ATPase residues 374–392 and 457–468, which correspond to two of these surface loops. Ca^{2+}-ATPase residues 397–402 compose a specific interaction site for phospholamban (Toyofuku et al., 1994), so it is not surprising that this structural feature is not

conserved in Na^+,K^+-ATPase. Ca^{2+}-ATPase residues 574–589 form a highly exposed "crown" helix preceded by an extended loop; although there is no corresponding deletion in the Na^+,K^+-ATPase sequence, this region shows no real homology and, in fact, is deleted in the corresponding H^+-ATPase and CadA sequences. Finally, the loop 428–433 corresponds to a three-residue insert in Na^+,K^+-ATPase, which is near its T1 tryptic cleavage site (R438) that is accessible in E_2 but not in E_1 (Jorgensen and Andersen, 1988). The protrusion of the latter two loops suggests that the corresponding Na^+,K^+-ATPase loops are either disordered or folded differently.

In addition to rearranging these cytoplasmic domains, this E_2-to-E_1 conformational change also induces a large displacement of the transmembrane domain relative to the P-domain (Fig. 7 *D*). After positioning the P-domain, an ~40° inclination and ~30° rotation is required to fit the transmembrane helices from the E_1 Ca^{2+}-ATPase crystal structure into the E_2 map of Na^+,K^+-ATPase (Fig. 7 *D*); a similar movement is required to match the E_2 map of Ca^{2+}-ATPase. In actuality, the membrane domain most likely remains fixed and the binding of Ca^{2+} or Na^+ induces the corresponding movement of the P-domain as well as an ~80° counter-rotation of the nose and an ~20° inclination of the N-domain, all of which serve to dissociate the cytoplasmic domains and provide wide-open access to the site of phosphorylation.

CONCLUSION

In summary, we have presented a structure of Na^+,K^+-ATPase at 11-Å resolution in the E_2 conformation. Three regions of the cytoplasmic domain (nose, N-, and P-domains) could be clearly seen and were arranged similarly to Ca^{2+}-ATPase in the E_2 conformation. This result indicates not only that Na^+,K^+-ATPase has a similar architecture to Ca^{2+}-ATPase but also that the conformational changes previously postulated to couple nucleotide and ion sites are likely to occur in all P-type ATPases. In particular, the E_2 conformation appears to consist of a compact arrangement of cytoplasmic domains, whereas binding of the primary ion (e.g., Na^+ or Ca^{2+}) induces the E_1 conformation, thus loosening the association between these domains. This results in large inclinations and rotations of intact domains without apparently altering the arrangement of secondary structure within the domains; results from spectroscopy, chemical modification, and proteolysis of both Na^+,K^+-ATPase and Ca^{2+}-ATPase are consistent with such changes. By fitting the atomic coordinates for Ca^{2+}-ATPase in the E_1 conformation to our map of Na^+,K^+-ATPase in the E_2 conformation, we correlated most of the variable parts of the sequence with surface-exposed loops. Also, it was apparent that the conformational change involved a large inclination and rotation of the phosphorylation domain relative to the transmembrane domain. Although we could not resolve individual helices within the membrane, our structure allowed us to postulate the location of the β-subunit transmembrane helix near α-subunit helices M7 and M10. In addition, the extracellular portion of β may have two sites of interaction with the α subunit. In future work we will increase the number of images included in our reconstruction in an attempt to improve resolution. Such a strategy has been successful for Ca^{2+}-ATPase, which improved from 14 to 8 Å with a fivefold increase in the number of tubes (Zhang et al., 1998), and nicotinic acetylcholine receptor, which has been defined to 4.6 Å (Miyazawa et al., 1999). For Na^+,K^+-ATPase, we hope that the next step will reveal the packing of membrane-spanning helices and will better define the interaction between α and β subunits.

We thank N. Unwin for the use of programs for helical image analysis, C. Toyoshima for the use of programs for CTF estimation, and S. Darst for the use of programs for helical re-indexing.

This work was supported by National Institutes of Health grants GM56960 (D.L.S.) and DK19185 (J.R.S.). W.J.R. was supported by a postdoctoral fellowship from the Human Frontier Science Program. H.S.Y. was supported by a Scientist Development grant from the American Heart Association, Heritage Affiliate.

REFERENCES

Abriel, H., U. Hasler, K. Geering, and J. D. Horisberger. 1999. Role of the intracellular domain of the beta subunit in Na,K pump function. *Biochim. Biophys. Acta.* 1418:85–96.

Beroukhim, R., and N. Unwin. 1997. Distortion correction of tubular crystals: improvements in the acetylcholine receptor structure. *Ultramicroscopy.* 70:57–81.

Cantley, L. C., Jr., L. G. Cantley, and L. Josephson. 1978. A characterization of vanadate interactions with the (Na,K)-ATPase: mechanistic and regulatory implications. *J. Biol. Chem.* 253:7361–7368.

Colonna, T. E., L. Huynh, and D. M. Fambrough. 1997. Subunit interactions in the Na,K-ATPase explored with the yeast two-hybrid system. *J. Biol. Chem.* 272:12366–12372.

DeRosier, D. J., and P. B. Moore. 1970. Reconstruction of three-dimensional images from electron micrographs of structures with helical symmetry. *J. Mol. Biol.* 52:355–369.

DeRosier, D., D. L. Stokes, and S. A. Darst. 1999. Averaging data derived from images of helical structures with different symmetries. *J. Mol. Biol.* 289:159–165.

Gadsby, D. C., R. F. Rakowski, and P. De Weer. 1993. Extracellular access to the Na,K pump: pathway similar to ion channel. *Science.* 260: 100–103.

Glynn, I. M. 1985. The Na^+,K^+-transporting adenosine triphosphatase. *In* The Enzymes of Biological Membranes. A. N. Martonosi, editor. Plenum Press, New York. 35–114.

Goldshleger, R., and S. J. Karlish. 1999. The energy transduction mechanism of Na,K-ATPase studied with iron-catalyzed oxidative cleavage. *J. Biol. Chem.* 274:16213–16221.

Hasler, U., X. Wang, G. Crambert, P. Beguin, F. Jaisser, J. D. Horisberger, and K. Geering. 1998. Role of beta-subunit domains in the assembly, stable expression, intracellular routing, and functional properties of Na,K-ATPase. *J. Biol. Chem.* 273:30826–30835.

Hebert, H., E. Skriver, and A. B. Maunsbach. 1985. Three-dimensional structure of renal Na,K-ATPase determined by electron microscopy of membrane crystals. *FEBS Lett.* 187:182–186.

Hebert, H., E. Skriver, M. Soderholm, and A. B. Maunsbach. 1988. Three-dimensional structure of renal Na,K-ATPase determined from two-dimensional membrane crystals of the p1 form. *J. Ultrastruct. Mol. Struct. Res.* 100:86–93.

Jencks, W. P. 1989. How does a calcium pump pump calcium? *J. Biol. Chem.* 264:18855–18858.

Jones, T. A., J. Y. Zou, S. W. Cowan, and M. Kjeldgaard. 1991. Improved methods for binding protein models in electron density maps and the location of errors in these models. *Acta Crystallogr. A.* 47:110–119.

Jorgensen, P. L. 1975. Purification and characterization of (Na^+,K^+)-ATPase. V. Conformational changes in the enzyme: transitions between the Na-form and the K-form studied with tryptic digestion as a tool. *Biochim. Biophys. Acta.* 401:399–415.

Jorgensen, P. L., and J. P. Andersen. 1988. Structural basis for E_1-E_2 conformational transitions in Na,K-pump and Ca-pump proteins. *J. Membr. Biol.* 103:95–120.

Jorgensen, P. L., and I. Klodos. 1978. Purification and characterization of $(Na^+ + K^+)$-ATPase. VII. Tryptic degradation of the Na-form of the enzyme protein resulting in selective modification of dephosphorylation reactions of the $(Na^+ + K^+)$-ATPase. *Biochim. Biophys. Acta.* 507: 8–16.

Kapakos, J. G., and M. Steinberg. 1982. Fluorescent labeling of $(Na^+ + K^+)$-ATPase by 5-iodoacetamidofluorescein. *Biochim. Biophys. Acta.* 693:493–496.

Karlish, S. J. 1980. Characterization of conformational changes in (Na,K) ATPase labeled with fluorescein at the active site. *J. Bioenerg. Biomembr.* 12:111–136.

Karlish, S. J., and D. W. Yates. 1978. Tryptophan fluorescence of $(Na^+ + K^+)$-ATPase as a tool for study of the enzyme mechanism. *Biochim. Biophys. Acta.* 527:115–130.

Kessi, J., J. C. Poiree, E. Wehrli, R. Bachofen, G. Semenza, and H. Hauser. 1994. Short-chain phosphatidylcholines as superior detergents in solubilizing membrane proteins and preserving biological activity. *Biochem.* 33:10825–10836.

Klug, A., F. H. C. Crick, and H. W. Wyckoff. 1958. Diffraction by helical structures. *Acta Cryst.* 11:199–213.

Koster, J. C., G. Blanco, and R. W. Mercer. 1995. A cytoplasmic region of the Na,K-ATPase alpha-subunit is necessary for specific alpha/alpha association. *J. Biol. Chem.* 270:14332–14339.

Kühlbrandt, W., M. Auer, and G. A. Scarborough. 1998. Structure of P-type ATPases. *Curr. Opin. Struct. Biol.* 8:510–516.

Lemas, M. V., M. Hamrick, K. Takeyasu, and D. M. Fambrough. 1994. 26 amino acids of an extracellular domain of the Na,K-ATPase alpha-subunit are sufficient for assembly with the Na,K-ATPase beta-subunit. *J. Biol. Chem.* 269:8255–8259.

Martin, D. W., and J. R. Sachs. 1999. Preparation of Na^+,K^+-ATPase with near maximal specific activity and phosphorylation capacity: evidence that the reaction mechanism involves all of the sites. *Biochemistry.* 38:7485–7897.

Miyazawa, A., Y. Fujiyoshi, M. Stowell, and N. Unwin. 1999. Nicotinic acetylcholine receptor at 4.6 Å resolution: transverse tunnels in the channel wall. *J. Mol. Biol.* 288:765–786.

Mohraz, M., M. V. Simpson, and P. R. Smith. 1987. The three-dimensional structure of the Na,K-ATPase from electron microscopy. *J. Cell. Biol.* 105:1–8.

Moller, J. V., B. Juul, and M. le Maire. 1996. Structural organization, ion transport, and energy transduction of ATPases. *Biochim. Biophys. Acta.* 1286:1–51.

Patchornik, G., R. Goldshleger, and S. J. Karlish. 2000. The complex ATP-Fe^{2+} serves as a specific affinity cleavage reagent in ATP-Mg^{2+} sites of Na,K-ATPase: altered ligation of Fe^{2+} (Mg^{2+}) ions accompanies the $E_1P \rightarrow E_2P$ conformational change. *Proc. Natl. Acad. Sci. U.S.A.* 97:11954–11959.

Sagara, Y., J. B. Wade, and G. Inesi. 1992. A conformational mechanism for formation of a dead-end complex by the sarcoplasmic reticulum ATPase with thapsigargin. *J. Biol. Chem.* 267:1286–1292.

Skou, J. C. 1957. The influence of some cations on an adenosine triphosphatase from peripheral nerves. *Biochim. Biophys. Acta.* 23:394–401.

Skriver, E., U. Kaveus, H. Hebert, and A. B. Maunsbach. 1992. Three-dimensional structure of Na,K-ATPase determined from membrane crystals induced by cobalt-tetrammine-ATP. *J. Struct. Biol.* 108: 176–185.

Skriver, E., A. B. Maunsbach, and P. L. Jorgensen. 1981. Formation of two-dimensional crystals in pure membrane-bound Na^+/K^+-ATPase. *FEBS Lett.* 131:219–222.

Stokes, D. L., M. Auer, P. Zhang, and W. Kuehlbrandt. 1999. Comparison of H^+-ATPase and Ca^{2+}-ATPase suggests that a large conformational change initiates P-type ion pump reaction cycles. *Curr. Biol.* 9:672–679.

Stokes, D. L., and N. M. Green. 2000. Modeling a dehalogenase fold into the 8-Å density map for Ca^{2+}-ATPase defines a new domain structure. *Biophys. J.* 78:1765–1776.

Stokes, D. L., and J.-J. Lacapere. 1994. Conformation of Ca^{2+}-ATPase in two crystal forms: effects of Ca^{2+}, thapsigargin, AMP-PCP, and Cr-ATP on crystallization. *J. Biol. Chem.* 269:11606–11613.

Toyofuku, T., K. Kurzydlowski, M. Tada, and D. H. MacLennan. 1994. Amino acids Lys-Asp-Asp-Lys-Pro-Val^{402} in the Ca^{2+}-ATPase of cardiac sarcoplasmic reticulum are critical for functional association with phospholamban. *J. Biol. Chem.* 269:22929–22932.

Toyoshima, C., M. Nakasako, H. Nomura, and H. Ogawa. 2000. Crystal structure of the calcium pump of sarcoplasmic reticulum at 2.6 Å resolution. *Nature.* 405:647–655.

Toyoshima, C., H. Sasabe, and D. L. Stokes. 1993a. Three-dimensional cryo-electron microscopy of the calcium ion pump in the sarcoplasmic reticulum membrane. *Nature.* 362:469–471.

Toyoshima, C., K. Yonekura, and H. Sasabe. 1993b. Contrast transfer for frozen-hydrated specimens. II. Amplitude contrast at very low frequencies. *Ultramicroscopy.* 48:165–176.

Unwin, N. 1993. Nicotinic acetylcholine receptor at 9 Å resolution. *J. Mol. Biol.* 229:1101–1124.

Wriggers, W., R. K. Agrawal, D. L. Drew, A. McCammon, and J. Frank. 2000. Domain motions of EF-G bound to the 70S ribosome: insights from a hand-shaking between multi-resolution structures. *Biophys. J.* 79:1670–1678.

Wriggers, W., R. A. Milligan, and J. A. McCammon. 1999. Situs: a package for docking crystal structures into low-resolution maps from electron microscopy. *J. Struct. Biol.* 125:185–195.

Yamashita, I., K. Hasegawa, H. Suzuki, F. Vonderviszt, Y. Mimori-Kiyosue, and K. Namba. 1998. Structure and switching of bacterial flagellar filaments studied by x-ray fiber diffraction. *Nat. Struct. Biol.* 5:125–32.

Yonekura, K., D. L. Stokes, H. Sasabe, and C. Toyoshima. 1997. The ATP-binding site of Ca^{2+}-ATPase revealed by electron image analysis. *Biophys. J.* 72:997–1005.

Zhang, P., C. Toyoshima, K. Yonekura, N. M. Green, and D. L. Stokes. 1998. Structure of the calcium pump from sarcoplasmic reticulum at 8 Å resolution. *Nature.* 392:835–839.